THE ASTROPHYSICAL JOURNAL, 546:825–828, 2001 January 10

A RADIO TELESCOPE SEARCH FOR AXIONS

B. D. BLOUT,[1] E. J. DAW,[1] M. P. DECOWSKI,[1] P. T. P. HO,[2] L. J ROSENBERG,[1] AND D. B. YU[1]
Received 2000 June 21; accepted 2000 August 17

ABSTRACT

The axion is a hypothetical elementary particle and a cold dark matter candidate. It could dominate the potential wells of most astrophysical objects. Axions spontaneously decay into nearly monochromatic microwave photons. We present results from a radio telescope search for these axion decay photons of mass $m_a = 298$–363 μeV in Local Group dwarf galaxies. We report a limit on the axion–to–two-photon coupling constant $g_{a\gamma\gamma} > 1.0 \times 10^{-9}$ GeV^{-1}.

Subject headings: dark matter — elementary particles — galaxies: dwarf — radio lines: general

1. INTRODUCTION

The axion is a hypothetical elementary particle, the pseudo-Goldstone boson associated with a Peccei-Quinn symmetry invoked to solve the "strong-CP problem" in QCD (Peccei & Quinn 1977; Weinberg 1978; Wilczek 1978). The axion is a good cold dark matter candidate (Kolb & Turner 1994); it could today dominate the potential wells of most astrophysical objects. The axion spontaneously decays into two photons with lifetime (Kolb & Turner 1994)

$$\tau_a = 6.8 \times 10^{24} \left(\frac{0.72}{E/N - 1.95}\right)^2 \left(\frac{m_a}{\text{eV}}\right)^{-5} \text{s}, \qquad (1)$$

where E/N is a model-dependent parameter. The search described here seeks a spectral line from axion decays in halos of Local Group dwarf galaxies.

There is a model range of perhaps a factor of 10 for the axion–to–two-photon coupling constant $g_{a\gamma\gamma}$ (Kim 1998). In two very different benchmark models, $g_{a\gamma\gamma}$ varies from about $1.35 \times 10^{-16}(m_a/\mu\text{eV})$ GeV^{-1} (the DFSZ model; Zhitnitsky 1980; Dine, Fischler & Srednicki 1981) to $3.65 \times 10^{-16}(m_a/\mu\text{eV})$ GeV^{-1} (the KSVZ model; Kim 1979; Shifman, Vainshtein, & Zakharov 1989). Various terrestrial experiments and astrophysical/cosmological arguments constrain the axion mass to the approximate window 10^{-6} to 10^{-3} eV, and $g_{a\gamma\gamma}$ to less than $\sim 1 \times 10^{-10}$ GeV^{-1} (Turner 1990). In one such astrophysical argument, leading to the "red giant limit" (Raffelt & Dearborn 1987), axions alter energy transport in red giants. An axion with $g_{a\gamma\gamma}$ greater than 1×10^{-10} GeV^{-1} would noticeably alter the abundances in the Hertzsprung-Russell horizontal branch. This limit, while the most sensitive in the upper two decades of the allowed axion mass window, does not reach the benchmark model sensitivities. Further, this limit depends on detailed models of red giant stellar evolution.

By contrast, the main assumption for this radio telescope search is that axions dominate potential wells. This search examines Local Group dwarf galaxies. If axions are present in these galaxies, then photons from their decay will appear as narrow lines in radio telescope power spectra (see Bershady, Ressell, & Turner 1991; this is a similar search applied to rich clusters using an optical telescope, closing the 3–8 eV axion window).

2. EXPECTED SIGNAL

An estimate of the expected axion signal requires three main input parameters: the spatial distribution of dark matter in a potential well, the particular axion model, and the axion mass. A halo axion can decay into two photons, each with frequency $\nu = (1/2)m_a c^2/h$ in the axion rest frame. The volume power density from axion decays in the halo is $P_V = (1/2)\rho_a c^2/\tau_a$, where ρ_a is the axion mass density and τ_a is the axion lifetime. Projecting P_V onto the sky gives the power per solid angle $P_S(\Omega)$.

The observed power from axion decays is then given by convolving $P_S(\Omega)$ with the beam pattern $B(\Omega)$ integrated over the surface A of the antenna:

$$P_{\text{obs}} = \int \frac{1}{4\pi D^2} P_S(\Omega) B(\Omega) dA\, d\Omega\,, \qquad (2)$$

where D is the distance from Earth to the galaxy. For the Haystack antenna in the 7 mm band, $B(\Omega)$ is a two-dimensional Gaussian with beamwidth 0.8 arcmin. The factors in equation (2) lead to the relation $P_{\text{obs}} \propto m_a^{\alpha}$ with $3 < \alpha < 5$. The value of the scaling parameter α depends on the source size and beamwidth. (The axion–to–two-photon coupling constant is proportional to the axion mass. If the source angular size is very small, then the beam pattern weighting in eq. [2] is constant. The observed power would then scale as m_a^5. If the source is diffuse, then eq. [2] approaches the integral of a two-dimensional Gaussian distribution. In this case the beam pattern is convolved with the nearly constant $P_S(\Omega)$, resulting in two additional factors of the wavelength.) An axion spectral line would appear with a Doppler-broadened width $\Delta\nu/\nu \sim \sigma_{\text{LOS}}/c$ where σ_{LOS} is the line-of-sight velocity dispersion within the object.

We modeled the halo mass distribution as an isothermal sphere (Chandrasekhar 1960) with radial mass density

$$9\rho(r) = \frac{9\sigma_{\text{LOS}}^2}{4\pi G(r^2 + a^2)}\,, \qquad (3)$$

where G is the gravitational constant, r is the radial distance from the object center, and a is the core radius (Binney & Tremaine 1989). This model includes a cutoff radius to avoid a divergent total mass. These results are only very weakly dependent on the choice of cutoff radius; we used

[1] Department of Physics and Laboratory for Nuclear Science, Massachusetts Institute of Technology, Cambridge, MA 02139.
[2] Harvard-Smithsonian Center for Astrophysics, Cambridge, MA 02138.

10*a*. There are other models with a steeper mass falloff (e.g., King 1966); the isothermal sphere model used here leads to the more conservative limit on the coupling constant.

We chose three Local Group dwarf galaxies for study: Pegasus, Leo I, and LGS 3 (see Mateo 1998 for sources Leo I [J1008+1218], LGS 3 [J0103+2153], and Pegasus [J2328+1444]). Dwarf galaxies were chosen because they have low virial velocities, resulting in a narrow signal line, $\delta v/v \sim 10^{-5}$, easily distinguishable from broader instrument-induced structure. Also, these objects have high mass-to-light ratios, and are likely dominated by dark matter. Further, these three galaxies are not known to be tidally disrupted (Burkert 1997), and the angular diameter of these galaxies—several arcminutes—is well matched to the antenna beamwidth.

3. OBSERVATIONS

Observations were made at Haystack Observatory (Westford, Massachusetts) on the 37 m radio telescope (see Ingalls et al. 1994) at frequencies from 35.92 to 44.08 GHz.

Each observation is an "off/on" background-subtracted power spectrum with a 160 MHz bandwidth. Each off/on spectrum was derived from two measurements. First, the telescope was pointed a small angle ahead of the object as it moved across the sky and a 30 s "off-source" background spectrum recorded. This off-source region of the sky has no known radio sources (see Madore et al. 2000) and represents the same section of the atmosphere and radome that will shortly be tracked with the target source. Second, the telescope was pointed at the object and a 30 s "on-source" spectrum recorded. Finally, the off-source spectrum subtracted from the on-source spectrum yielded the off/on spectrum. This off/on technique, in tracing the same arc of the sky and radome twice, minimizes terrestrial artifacts.

Before making an observation, the antenna temperature was calibrated with a blackbody load placed in front of the receiver feed horn. This calibration was repeated for every change in frequency, every change in observing object, and otherwise approximately every 10 minutes. This serves to calibrate the instrumental response as a function of frequency. Typical system temperatures were in the range 100–230 K.

There are two major sources of error. The first is "pointing error," the angular mismatch between commanded and actual antenna direction. From known sources, such as planets and quasars, the typical pointing error varied from negligible to 15″. For this analysis, we used a conservative fixed pointing error of 22″. A fully realized pointing error results in a signal power degradation of 35%, our dominant uncertainty.

The second source of error is uncertainty in the "efficiency" of the telescope, which represents all sources of signal attenuation. These include the atmosphere, scattering from the radome, and varying gravitational deformation of the antenna as the dish moves in elevation. Again from known sources, the typical efficiency is between 29% and 34%. For this analysis, we used a conservative constant efficiency of 27%.

4. RESULTS

Power spectra were collected at the Haystack Observatory on 1999 April 21, 1999 October 15, 1999 December 29–31, and 2000 March 21. The total number of spectra at any one frequency is at least three and sometimes more than 10. Higher numbers of observations were made for frequencies that contained unusual features or candidates. (As explained below, these have all been ruled out as axions.)

Each spectrum has a 160 MHz bandwidth and was derived from a 256 time-lag autocorrelation spectrometer. Thus, each bin has Nyquist width 625 kHz; the expected axion signal has a width of about two bins. The high- and low-frequency ends of some spectra show bandpass filter skirts, so the first and last quarters of the bins are removed from each spectrum. The remaining 80 MHz of data per spectrum are used for all subsequent analysis.

The baseline of each spectrum is estimated from a least-squares fit to a fourth-order polynomial. This estimated baseline is then subtracted from the spectrum. In Monte Carlo simulations, the order of the fitted polynomial improves the axion signal-to-noise ratio up to fourth order, after which the sensitivity changes little.

A typical background-subtracted power spectrum is shown in Figure 1. The vertical axis shows power spectral density, and the horizontal axis shows frequency. The ends of the spectrum have been removed, leaving the central 128 of the original 256 bins. The curve shows the fitted baseline. In addition, a simulated axion line of coupling strength $g_{a\gamma\gamma} = 1.2 \times 10^{-9}$ GeV^{-1} has been superimposed near the middle of the spectrum.

Bins from different spectra at the same frequency are combined into a weighted average, forming a "combined spectrum" (see Daw 1998; bins from different spectra are weighted by the inverse square of the corresponding spectrum noise temperature, and the combined spectrum noise temperature is the reciprocal square root of the sum of the weights). The combined spectrum for dwarf galaxy LGS 3 is shown in Figure 2. The spectrum shows the relatively large system noise temperature near 39 GHz.

Next, the combined spectrum was normalized using its noise temperature (Daw 1998). Figure 3 is a histogram of the deviations in the LGS 3 normalized combined spectrum. The line shows the expectation for unit-variance Gaussian noise.

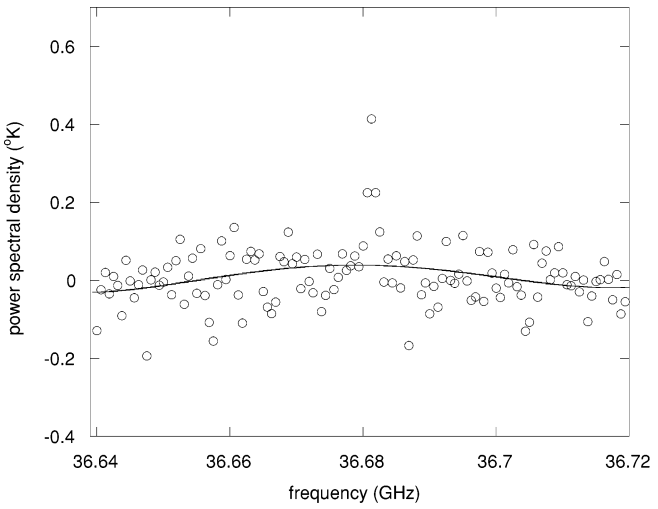

FIG. 1.—Typical background-subtracted power spectrum with filter skirts removed, plus a simulated axion line near 36.68 GHz. The curve shows the fitted baseline.

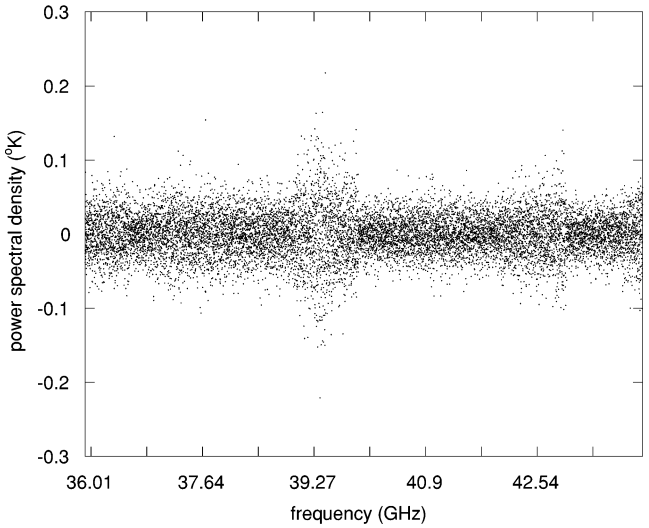

FIG. 2.—Combined background-subtracted power spectrum from dwarf galaxy LGS 3. The system noise temperature was relatively large near 39 GHz.

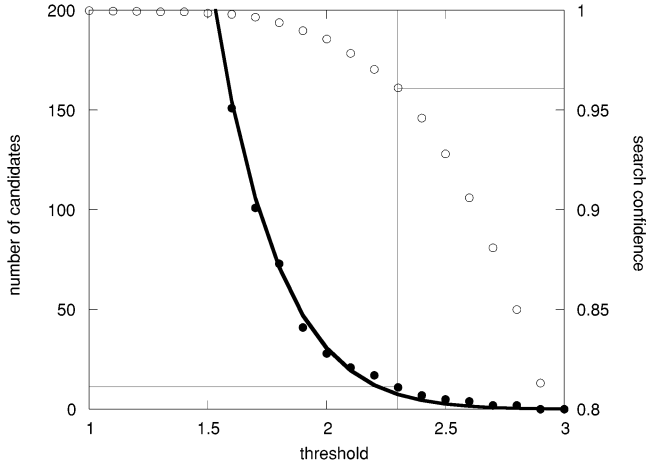

FIG. 4.—Number of candidates (*filled circles, left ordinate*) and search confidence (*open circles, right ordinate*) vs. threshold for LGS 3. The curve shows the expected number of candidates for unit-variance Gaussian noise. The horizontal axis is candidate threshold in units of standard deviations. The vertical line indicates the selected threshold; the horizontal lines show the resulting number of candidates and search confidence.

We formed a "candidate spectrum" by averaging every two adjacent bins of the normalized combined spectrum. Candidates are defined as those bins in the candidate spectrum exceeding a selected threshold. The filled circles in Figure 4 show the number of candidates (*left vertical axis*) versus threshold for LGS 3. The horizontal axis is threshold in units of the normalized combined spectrum's standard deviation. The curve shows the expected number of candidates versus threshold for unit-variance Gaussian noise.

From Figure 4 we selected a threshold of 2.3, resulting in 16 candidates. In Monte Carlo simulations we injected axion lines with varying power and the expected virial width into the unfitted spectra. We determined that an axion line of about 10^{-18} W gave a 96% search confidence at the selected threshold; this is the search power sensitivity, $P_{\rm sens}$. (Since the noise temperature varied across the spectrum, the power sensitivity varied as well to maintain a flat 96% search confidence.) The open circles in Figure 4 show the search confidence for axions injected with $P_{\rm sens}$. Like the red giant limit, this power sensitivity is much higher than that required to detect KSVZ axions.

An axion signal should always be present at a given frequency. We returned to Haystack Observatory on 2000 March 21 to examine the 16 candidates from LGS 3. We determined that in these later data the corresponding power for each candidate was small; this is consistent with the 16 candidates being noise fluctuations. We therefore eliminated all 16 candidates while maintaining overall search confidence at 96%.

$P_{\rm obs}$ for all three galaxies is approximately the same. However, the smaller angular size of LGS 3 yields better coupling constant sensitivity (through the scaling factor α). The search procedure for Leo I and Pegasus is identical to that for LGS 3, except that the power threshold is set high enough to exclude any candidates.

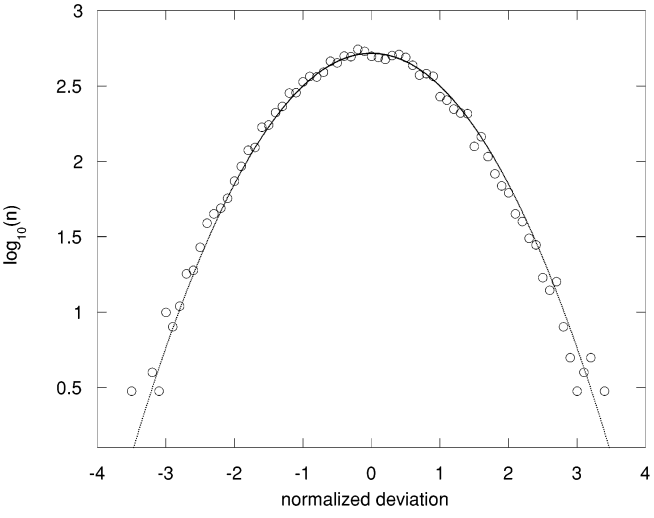

FIG. 3.—Histogram of the deviations in the normalized combined spectrum. The curve shows simulated Gaussian deviations of unit width normalized to the number of frequency bins (13,056).

5. COUPLING CONSTANT SENSITIVITY

The relation between measured and predicted (KSVZ) power and coupling constant sensitivity is

$$\frac{P_{\rm sens}}{P_{\rm KSVZ}} = \left(\frac{g_{\rm sens}}{g_{\rm KSVZ}}\right)^{\alpha}, \qquad (4)$$

where $P_{\rm sens}$ and $g_{\rm sens}$ are the axion power and coupling constant sensitivity of this search; α is that of § 2; and $P_{\rm KSVZ}$ is obtained from equation (2).

Figure 5 shows α as a function of frequency for LGS 3, Leo I, and Pegasus. As frequency increases, the beamwidth of the antenna narrows, the source looks relatively more diffuse, and α decreases.

The excluded values of the axion–to–two-photon coupling constant at 96% search confidence for LGS 3, Leo I, and Pegasus are shown in Figure 6. The lower horizontal axis is the photon frequency, and the upper horizontal axis

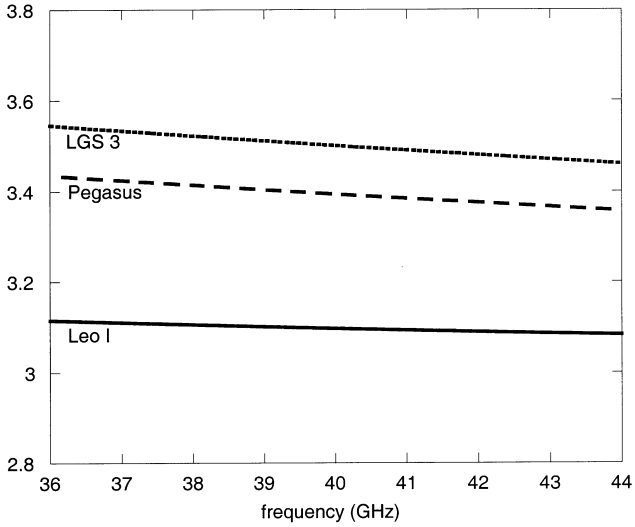

FIG. 5.—Scaling factor α in the power law $P \propto m^{\alpha}$ for LGS 3 (*dotted line*), Pegasus (*dashed line*), and Leo I (*solid line*). The factor α varies with the antenna beamwidth and source angular size.

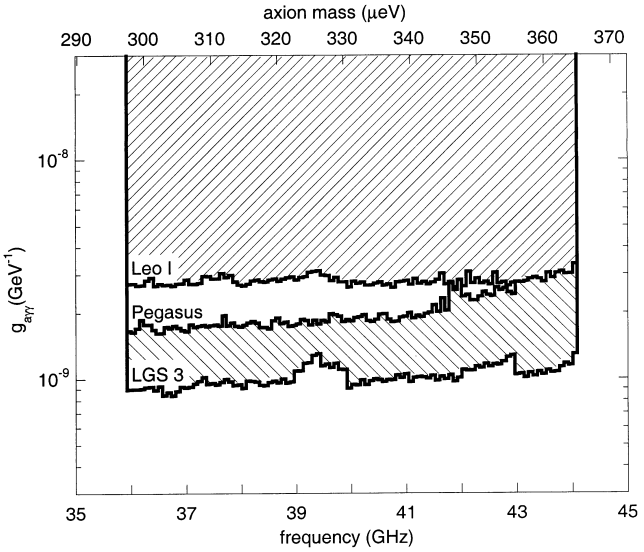

FIG. 6.—Excluded axion–to–two-photon coupling $g_{a\gamma\gamma}$ vs. photon frequency (*lower abscissa*) and axion mass (*upper abscissa*) for the sources LGS 3, Pegasus, and Leo I.

is the corresponding axion mass. The vertical axis shows the excluded coupling constant $g_{a\gamma\gamma}$. The sensitivity varies with the receiver noise and source. We excluded axion–to–two-photon coupling constants of 1.0×10^{-9} GeV^{-1} or greater.

6. CONCLUSIONS

This search ruled out axions of mass 298–363 μeV with axion–to–two-photon coupling of $g_{a\gamma\gamma} > 1.0 \times 10^{-9}$ GeV^{-1} at 96% confidence. For the first time, a radio telescope was used to search for cold dark matter axions in the allowed mass window.

The sensitivity of this result is comparable to the red giant limit. However, the assumptions are very different; the radio telescope technique does not rely on detailed models of stellar evolution.

The radio frequency cavity axion search technique (Sikivie 1983) achieves remarkable sensitivity at the lower axion masses. Radio telescopes are more suited to search for axions of higher mass. Present radio telescope technology allows searches to the very upper end of the allowed axion mass window at sensitivities comparable to this result.

We are grateful to the research staff of Haystack Observatory for the use of the facility and for helpful discussions. In particular, we thank J. Ball, P. Pratap, and P. A. Shute for their guidance. We also thank J. Hewitt for her many helpful suggestions. Support for the use of the Haystack telescope was provided by the National Science Foundation under grant DUE-9952246.

REFERENCES

Bershady, M. A., Ressell, M. T., & Turner, M. S. 1991, Phys. Rev. Lett., 66, 1398
Binney, J., & Tremaine, S. 1989, Galactic Dynamics (Princeton: Princeton Univ. Press)
Burkert, A. 1997, ApJ, 474, L99
Chandrasekhar, S. 1960, Principles of Stellar Dynamics (New York: Dover)
Daw, E. 1998, Ph.D. thesis, MIT
Dine, M., Fischler, W., & Srednicki, M. 1981, Phys. Lett., B104, 199
Ingalls, R. P., et al. 1994, Proc. IEEE, 82, 742
Kim, J. E. 1979, Phys. Rev. Lett., 43, 103
———. 1998, Phys. Rev. D, 58, 055006
King, I. R. 1966, AJ, 71, 64
Kolb, E. W., & Turner, M. S. 1994, The Early Universe (Reading: Addison-Wesley)
Madore, B., et al. 2000, NASA/IPAC Extragalactic Database (NED) (Pasadena: JPL)
Mateo, M. 1998, ARA&A, 36, 435
Peccei, R. D., & Quinn, H. R. 1977, Phys. Rev. Lett., 38, 1440
Raffelt, G. G., & Dearborn, D. S. P. 1987, Phys. Rev. D, 36, 2211
Shifman, M. A., Vainshtein, A. I., & Zakharov, V. I. 1980, Nucl. Phys. B, 166, 493
Sikivie, P. 1983, Phys. Rev. Lett., 51, 1415
Turner, M. S. 1990, Phys. Rep., 197, 67
Weinberg, S. 1978, Phys. Rev. Lett., 40, 223
Wilczek, F. 1978, Phys. Rev. Lett., 40, 279
Zhitnitsky, A. R. 1980, Soviet J. Nucl. Phys., 31, 260